

T. Song, R. Bachelet, G. Saint-Girons, R. Solanas, I. Fina, and F. Sánchez, ACS Appl. Electron. Mater. 2, 3221-3232 (2020)
<https://pubs.acs.org/doi/10.1021/acsaelm.0c00560>

The Supporting Information is available free of charge at <https://pubs.acs.org/doi/10.1021/acsaelm.0c00560>.

Epitaxial Ferroelectric La-doped $\text{Hf}_{0.5}\text{Zr}_{0.5}\text{O}_2$ Thin Films

Tingfeng Song,¹ Romain Bachelet,² Guillaume Saint-Girons,² Raul Solanas,¹ Ignasi Fina,^{1,*}
Florencio Sánchez^{1,*}

¹ Institut de Ciència de Materials de Barcelona (ICMAB-CSIC), Campus UAB, Bellaterra 08193, Barcelona, Spain

² Institut des Nanotechnologies de Lyon (INL-CNRS UMR 5270), Université de Lyon, Ecole Centrale de Lyon, 36 avenue Guy de Collongue, 69134 Ecully Cedex, France.

ABSTRACT

Doping ferroelectric $\text{Hf}_{0.5}\text{Zr}_{0.5}\text{O}_2$ with La is a promising route to improve endurance. However, the beneficial effect of La on the endurance of polycrystalline films may be accompanied by degradation of the retention. We have investigated the endurance - retention dilemma in La-doped epitaxial films. Compared to undoped epitaxial films, large values of polarization are obtained in a wider thickness range, whereas the coercive fields are similar, and the leakage current is substantially reduced. Compared to polycrystalline La-doped films, epitaxial La-doped films show more fatigue but there is not significant wake-up effect and endurance-retention dilemma. The persistent wake-up effect common to polycrystalline La-doped $\text{Hf}_{0.5}\text{Zr}_{0.5}\text{O}_2$ films, is limited to a few cycles in epitaxial films. Despite fatigue, endurance in epitaxial La-doped films is more than 10^{10} cycles, and this good property is accompanied by excellent retention of more than 10 years. These results demonstrate that wake-up effect and endurance-retention dilemma are not intrinsic in La-doped $\text{Hf}_{0.5}\text{Zr}_{0.5}\text{O}_2$.

INTRODUCTION

Stabilization of the metastable orthorhombic (o) ferroelectric phase in doped HfO₂ films¹ can have a great technological impact. HfO₂ films can be grown by atomic layer deposition, a process compatible with CMOS technology, and can overcome the lack of scalability of conventional ferroelectric oxides.²⁻⁴ Ferroelectric hafnia holds promise for non-volatile random access devices, but also for emerging ferroelectric memories such as tunnel junctions and field effect transistors. However, the endurance of HfO₂ capacitors, which is a critical property for memory devices, is moderately low. The low endurance of ferroelectric HfO₂ is perhaps the consequence of a large coercive field (E_c), >1 MV/cm, around one order of magnitude greater than that of perovskite oxides. The electric field required to cycle HfO₂ is very high, close to the breakdown field, and endurance of HfO₂ capacitors is generally limited by hard breakdown that usually occurs well below 10^{10} cycles.

Doping with trivalent La atoms has allowed a significant improvement. In particular, Hf_{0.5}Zr_{0.5}O₂ (HZO) films doped with 1 mol% La show increased polarization and endurance up to 4×10^{10} cycles.⁵ This was accomplished by reducing E_c and leakage current by around 30% and three orders of magnitude, respectively.⁵ Optimizing the amount of La has allowed a further enhancement.⁶ HZO capacitors doped with 0.7 mol% La remained operational after 10^{11} cycles, and without polarization reduction (fatigue).⁶ However, optimization of endurance by La-doping can be accompanied by a severe degradation of polarization retention.⁷ The endurance of films doped with 2.5 mol% La, the optimal amount considering all ferroelectric properties, was only 10^7 cycles. On the other hand, a common detrimental effect of La doping is the highly increased wake-up effect up to $10^5 - 10^7$ cycles.⁵⁻⁷

Studies on the effects of doping with La have been carried out with polycrystalline films. Ferroelectricity has been reported for epitaxial films of HfO₂ doped with several atoms, including Y,⁸⁻⁹ Zr,¹⁰⁻²⁴ and Si.²⁵ The remanent polarization (P_r) in epitaxial films can exceed $20 \mu\text{C}/\text{cm}^2$, and the E_c is greater than in polycrystalline samples.^{10-17, 22-25} In addition, the usual E_c - thickness (t) scaling in conventional ferroelectric perovskites, $E_c \propto t^{-2/3}$,²⁶⁻²⁷ elusive in polycrystalline HZO or other doped-HfO₂ films, is observed in epitaxial HZO films.^{15, 22} Endurance of epitaxial HZO films can be high in spite of their enormous E_c of 3-4 MV/cm.^{10, 14, 16, 22} Indeed, endurance of 10^{11} cycles

has been measured in sub-5 nm HZO films applying a very large electric field above 5 MV/cm.²² Further improvement could be achieved by decreasing leakage and the huge E_c of epitaxial films. By doping with La, an acceptor dopant for HZO, it has been possible to reduce leakage and E_c in polycrystalline HZO films and, therefore, it is of great interest to stabilize the o-phase in epitaxial La-doped HZO (La:HZO) films, and measure ferroelectric polarization, endurance and retention. In order to investigate the effects of La-doping in epitaxial films, we fixed the La content to the same amount (1 mol% La) that in the pioneering study by Chernikova et al.,⁵ and La-doped HZO epitaxial films were deposited using growth conditions, substrates and bottom electrode suitable to stabilize the o-phase in undoped HZO films.

Epitaxial La:HZO films of thickness (t) in the 4.5 - 13 nm range were deposited on (001)-oriented SrTiO₃ (STO) substrates buffered with a La_{2/3}Sr_{1/3}MnO₃ (LSMO) electrode. The o-phase is epitaxially stabilized, and the films have P_r up to $\sim 28 \mu\text{C}/\text{cm}^2$, and E_c that scales with thickness according to the $\propto t^{2/3}$ dependence. Compared to undoped HZO epitaxial films of same thickness, E_c values are similar, while leakage current reduces by around one order of magnitude. Endurance improves over equivalent undoped epitaxial films, with strong thickness dependence in both doped and undoped films. Moreover, wake-up effect (100 cycles), hardly observed in epitaxial undoped HZO films, is evident in films thinner than around 8 nm although being it much less than for polycrystalline La:HZO. Films $t < 10$ nm show $2P_r > 2 \mu\text{C}/\text{cm}^2$ after 10^{10} cycles at field 4-5 MV/cm. Remarkably, high endurance is accompanied by long retention of more than 10 years using the same poling field. This demonstrates that high endurance and long retention can be attained simultaneously in La:HZO films on LSMO/STO(001). However, since Si wafers are required for applications, epitaxial La:HZO films were also grown on LSMO/STO/Si(001). LSMO and STO were grown by pulsed laser deposition (PLD) and molecular beam epitaxy (MBE), respectively. We note that STO and other perovskites can also be integrated epitaxially on Si(001) by atomic layer deposition, allowing for conformal deposition.²⁸ The epitaxial HZO films on Si(001) also exhibit high polarization, endurance and retention.

EXPERIMENTAL

La-doped and undoped HZO films were grown on LSMO/STO(001) and LSMO/STO/Si(001). The STO(001) single crystalline substrates were used in as-received conditions, thus presenting a majority of TiO₂ chemical terminations and minority of SrO.²⁹ The STO buffer layers, 26 nm thick, were grown *ex-situ* by molecular beam epitaxy (MBE). Additional information about MBE deposition of STO and its structural properties is reported elsewhere.¹⁶ HZO (doped and undoped) and LSMO films were grown in a single process by pulsed laser deposition (PLD) using a KrF excimer laser. The laser frequency was 5 and 2 Hz for LSMO and HZO, respectively. The composition of the PLD targets was Hf_{0.5}Zr_{0.49}La_{0.01}O₂, Hf_{0.5}Zr_{0.5}O₂ and La_{2/3}Sr_{1/3}MnO₃. Deposition was done under dynamic oxygen pressure of 0.1 mbar at 700 °C and 800 °C (heater block temperature) for LSMO and HZO, respectively. LSMO layer is used as bottom electrode with t = 25 nm thick, and HZO films are in the t = 4.5 - 13 nm range, being HZO thickness determined by the number of laser pulses used in the PLD process. At the end of the deposition, samples were cooled under 0.2 mbar oxygen pressure. Capacitors were fabricated chosen platinum, which can be deposited at room temperature, as top electrode. Pt circular top electrodes, of diameter 20 μm and thickness 20 nm, deposited by sputtering through stencil masks.

Crystal structure was studied by X-ray diffraction (XRD) with Cu K α radiation using a Siemens D5000 diffractometer equipped with point detector, and a Bruker D8-Advance diffractometer equipped with 2D detector. Surface topography was studied using atomic force microscopy (AFM) using a Keysight 5100. Ferroelectric polarization loops were measured using an AixACCT TFAAnalyser2000 platform at 1 kHz by the dynamic leakage current compensation (DLCC) procedure³⁰⁻³¹ at room temperature in top-bottom configuration. By DLCC method, the leakage current effects is suppressed based on two assumptions: that the leakage current is frequency independent and that the dielectric current (including ferroelectric switching current) is linearly dependent on the frequency. Therefore, leakage contribution to measured current can be subtracted by measuring cycles at two different frequencies (ν and $\nu/2$), and subtracting frequency independent current contribution. Endurance was measured cycling the sample at frequency of 100 kHz using bipolar square pulses of indicated amplitude and measuring polarization loops at 1 kHz. Retention was measured poling the sample using triangular pulse of 0.25 ms and determining the P_r from the first polarization curve of the polarization loop measured at 1kHz using the PUND protocol after a delay time.³¹

RESULTS

Figure 1a shows the XRD θ - 2θ scans of the La:HZO/LSMO/STO(001) samples. For clarity, the scans are vertically shifted, increasing HZO thickness from bottom to top. Besides the (001) and (002) reflections of the STO substrate and LSMO electrode, there is a peak at 2θ around 30° , coincident with the position of the o-HZO(111) reflection in epitaxial undoped HZO films.¹⁵ A zoomed 2θ range around this peak, scanned with longer acquisition time, is in the right panel of Figure 1a. Increasing thickness, the o-HZO(111) peak becomes narrower and Laue oscillations are evident. The thickness of the thickest film, calculated by simulation of the Laue oscillations (Supporting information S1) is 13.1 nm. The simulation shows an asymmetry, with the satellites being more intense at lower angles than at higher angles with respect to the o-HZO(111) peak. Asymmetry is observed in similar undoped epitaxial HZO(111) films.^{13,15} Laue oscillations around LSMO reflections are not observed due to the LSMO thickness (25 nm) and the measurement with Cu $K\alpha$ radiation that included Cu $K\alpha_1$ and Cu $K\alpha_2$ components. Pole figures (Supporting information S2) confirm epitaxy, with four in-plane crystal variants and same epitaxial relationship as the films without La.^{10, 15, 17, 21} Very low intensity peaks barely distinguished at $2\theta=34^\circ$ in Figure 1a, are likely m-HZO{200} reflections. XRD 2θ - χ frames (Supporting information S3) show intense o-HZO(111) spots, while the monoclinic reflections are not detected. This signals very low amount of monoclinic phase in epitaxial La:HZO films, smaller than the observed in equivalent epitaxial undoped HZO films.^{15, 17, 21} Similar reduction of monoclinic phase was observed in polycrystalline La-doped HZO films.^{5, 7} In summary, XRD confirms that the orthorhombic phase present in the La-doped HZO films has grown epitaxially, but exhibits crystal variants and coexists with a minority monoclinic phase. Therefore, the films are not monocrystalline: the majority orthorhombic phase presents crystal variants and coexists with the minority monoclinic phase, existing grain boundaries between crystal variants and between the two phases.

XRD θ - 2θ scans of the La:HZO/LSMO/STO/Si(001) samples (Figure 1b) confirm that the orthorhombic phase is also stabilized on Si(001). There are Laue oscillations around the o-HZO(111) peak (see right panel in Figure 1b and Supporting Information S1). Traces of m-HZO{200} reflections are more evident in these films than on STO(001), and the 2θ - χ frames

(Supporting information S3) recorded for the thicker films show elongated low intensity m -HZO{200} spots. Next, we determined the out-of-plane (oop) lattice parameter of the orthorhombic phase, $d_{o\text{-HZO}(111)}$, from the position of the o -HZO(111) peak in the θ - 2θ scans (Figures 1a and 1b). The dependence of $d_{o\text{-HZO}(111)}$ on thickness is represented in Figure 1c, for films on STO(001) (red triangles) and Si(001) (black squares). In both series, the oop parameter decreases slightly with t up to $t \sim 8$ nm, and the value remains constant in the thicker film ($t \sim 13$ nm). Similar dependence (blue squares) was found for undoped HZO films on STO(001).¹⁵ The smaller $d_{o\text{-HZO}(111)}$ values of the films on Si(001) respect the equivalent films on STO(001) is a consequence of the large mismatch in thermal expansion coefficients between the oxides and silicon. Due to the much smaller thermal expansion coefficient of Si, HZO will be under in-plane tensile stress when cooled after deposition, causing contraction of the out-of-plane $d_{o\text{-HZO}(111)}$ parameter. The oop parameters of the La-doped and undoped HZO films on Si(001) are quite similar, with slightly higher values in the series of doped films. The higher $d_{o\text{-HZO}(111)}$ in La doped films differs from the reported slight shrinkage for polycrystalline HZO films doped with similar La content.^{5, 7}

The surface of the films is very flat. The atomic force microscopy (AFM) topographic images of La:HZO films on STO(001) (Figure 2) show terraces and steps morphology. This morphology is more evident in the $t = 8.3$ nm, which presents the narrower terraces (130 wide in average). The root-means-square (rms) roughness is below 0.2 nm in all samples. Thinner films have high density of two-dimensional islands near the upper steps (see zooms in the insets of Figures 2a and 2b). Two-dimensional islands are not observed in thicker films, although the surface of these films remains very flat and the line topographic profiles show height variation of less than 1 nm over a distance of 5 μm (Supporting Information S4). Terraces are not distinguished in films on Si(001) (Supporting Information S5), but they are very flat, with rms around 0.2 - 0.3 nm, and height profiles within a range of 2 nm along a distance of 5 μm .

Figure 3a shows polarization loops of the films on STO(001). The loops were measured by the DLCC method (see Experimental Section), and thus they include ferroelectric and dielectric contributions, the latter causing the slope evident at high fields. All films are ferroelectric, with remanent polarization P_r in the 20-30 $\mu\text{C}/\text{cm}^2$ range. Due to the low thickness of the films and the large electric field applied, there is an influence of leakage, particularly for the $t = 4.8$ nm film and

positive voltage. The effect of leakage is twofold: it can add to switching current and polarization can be overestimated, but on the contrary, it does not allow full saturation of the loop and therefore the polarization is underestimated. Polarization loops measured at increasing voltage (Supporting Information S6) confirm that leakage is less prominent while increasing thickness and the loops are saturated for high-applied voltage. In addition, residual leakage subtraction performed using reported equations³² shows that its contribution is $2 \mu\text{C}/\text{cm}^2$, which is taken as a sensitivity limit (Supporting Information S7). Remanent polarization is represented in Figure 3b (blue solid up triangles) as a function of thickness. P_r is $\sim 20 \mu\text{C}/\text{cm}^2$ in the thinner film, $t = 4.8 \text{ nm}$, increases to $\sim 28 \mu\text{C}/\text{cm}^2$ in the $t = 6.2 \text{ nm}$ film, and for thicker films reduces with thickness up to $\sim 21 \mu\text{C}/\text{cm}^2$ in the $t = 13 \text{ nm}$ film. Figure 3b includes P_r values (green squares) of equivalent epitaxial undoped HZO films on STO(001)¹⁵ Both series show the same dependence on thickness, with a maximum polarization for films thinner than 10 nm, and having La-doped films slightly higher P_r than undoped films. Both series show the same dependence on thickness, with a maximum polarization for films thinner than 10 nm, and having La-doped films higher P_r than undoped films.

The polarization loops of the films on Si(001) are presented in Figure 3c. Loops corresponding to thinner films are not saturated due to leakage (see measurements at varying maximum voltage in Supporting Information S8). Remanent polarization P_r decreases monotonically with thickness (solid red down triangles in Figure 3b) from $>30 \mu\text{C}/\text{cm}^2$ to $21 \mu\text{C}/\text{cm}^2$. Similar high P_r in $t < 10 \text{ nm}$ films was reported for undoped HZO films integrated epitaxially on Si(001) using yttria-stabilized zirconia (YSZ) buffer layers (pink open circles in Figure 3b).²² Polarization decreases with thickness for both doped and undoped HZO films, but the reduction is less for La-doped films. Figure 3b also shows for films on STO(001) that the reduction of polarization with thickness in films thicker than around 10 nm is less for La-doped films than for undoped ones. The higher remanent polarization in thicker films could be due to the lower amount of monoclinic phase in La-doped HZO films. Undoped HZO films with very large remanent polarization were also integrated epitaxially on STO buffered Si(001) wafers, but the dependence on thickness was not reported¹⁶ The P_r value reported for a $t \sim 8 \text{ nm}$ HZO film is included in Figure 3b (orange diamond).

The E_c of the La:HZO films (Figures 3a and 3c) is very large. E_c is represented as a function of thickness in Figure 3d. As thickness increases from 4.8 to 13 nm, E_c decreases from 3.7 to 2.3

MV/cm in films on STO(001) (blue up triangles), and from 4.2 to 2.5 MV/cm in films on Si(001) (red down triangles). E_c of films on both substrates depends on thickness following the $E_c \propto t^{-2/3}$ scaling law. This phenomenological law is common in ferroelectric perovskites,³³ but is not observed in polycrystalline ferroelectrics based on HfO₂, which generally show little thickness dependence.³⁴ The $E_c \propto t^{-2/3}$ scaling has been also reported for epitaxial undoped HZO films.^{15, 22} We note that coercive field of both La-doped and undoped epitaxial HZO films is higher than that of equivalent polycrystalline films, being the difference higher for thinner films as polycrystalline films show little thickness dependence. We include in Figure 3d reported data for epitaxial HZO films on STO(001) (green squares) and YSZ buffered Si(001) (pink circles). E_c is seen to be greater in doped HZO films than in undoped HZO films. This is in contrast to the reduction of E_c by approximately 30% in polycrystalline HZO films doped with same 1% mol La content.⁵⁻⁶ Although the cause of E_c reduction in polycrystalline La doped films is unknown, the possible presence of tetragonal phase was suggested,⁶ but this phase apparently is not present in the epitaxial films on LSMO(001) electrodes.

Leakage current curves for La-doped HZO films on STO(001) are shown in Figures 4a. Leakage is low, even in the sub-5 nm film, which is around 10^{-6} A/cm² at 1 MV/cm and 10^{-5} A/cm² at 2 MV/cm. Leakage decreases with film thickness, and the values in the $t = 13$ nm film are about one order of magnitude less than in the $t = 4.8$ nm film. Films on Si(001) are slightly more leaky, with the leakage current of the thinner film around 3×10^{-6} A/cm² at 1 MV/cm and 5×10^{-5} A/cm² at 2 MV/cm. Similarly to the films on STO(001), leakage is significantly reduced with thickness. Figure 4c shows the thickness dependence of the current leakage at 2 MV/cm of films on STO(001) (blue up triangles) and Si(001) (red down triangles). The graph also includes leakage data from equivalent epitaxial undoped HZO films on STO(001) (green squares).¹⁵ It is observed that the leakage current of epitaxial La-doped HZO films is considerably reduced, 1 - 2 orders of magnitude, compared to equivalent undoped HZO films.

Figure 5 shows the current-voltage (I-V) curves and the polarization loops of the films on STO(001), in pristine state and measured after 10 and 100 cycles. The $t = 4.8$ nm film shows in pristine state a double peak in the I-V curve (Figure 5a) and a pinched polarization loop (Figure 5b). The two peaks get closer after 10 cycles, and after 100 cycles, they merge in a single narrower peak, and the corresponding polarization loop is not pinched. In the $t = 6.3$ nm film (Figure 5c),

the two peaks are closer in the pristine state, and after 10 pulses, only a small secondary peak on the positive axis is distinguished at a higher voltage than the main peak. With more cycles, the amplitude of the main peak has not changed, while the second peak has disappeared. The corresponding ferroelectric loops (Figure 5d) show a significant increase of polarization with respect to the pristine state. In contrast, no differences in the I-V curves were observed between the pristine state and the 10 times cycled $t = 8.3$ nm film (Figure 5e). There is a single peak that features a shoulder on the higher voltage side. The switching peak has a similar amplitude after 100 cycles, but without shoulder. Consistent with this, the polarization loops (Figure 5f) show no significant differences and there is only a very slight reduction in polarization after 100 cycles. Finally, in the thickest film, $t = 13$ nm, there is a single peak in the pristine state, which decreases in amplitude by cycling (Figure 5g). The resulting polarization loops (Figure 5h) show a reduction in remanent polarization with cycling. Therefore, the behavior of epitaxial La:HZO films with cycling is highly dependent on thickness. The two thinnest epitaxial films on Si(001) show a similar wake-up effect (Figure 6). The wake-up effect, which occurs recurrently in polycrystalline hafnia films, does not occur in epitaxial La:HZO films thicker than about 8 nm. In contrast, the films $t = 6.3$ and 4.8 nm waken after around 10 and 100 cycles, respectively. The wake-up effect is more evident than in same thickness epitaxial undoped HZO films, where the effect is less evident. In La-doped polycrystalline HZO films, wake-up effect increases strongly compared to undoped films.⁵⁻⁷ Indeed, wake-up effect in polycrystalline La-doped HZO films can extend to a larger number of about 10^7 cycles,⁶ which is one of the main drawbacks of La-doped HZO films. Therefore, the strong reduction or suppression of wake-up effect in epitaxial La:HZO films with respect to polycrystalline La:HZO films is relevant.

Next, we investigate the endurance of the films. The capacitors were cycled, up to a maximum number of 5×10^{10} cycles, or until breakdown (denoted by empty symbols) or a fatigued state with remanent polarization reduced to below $1.5 \mu\text{C}/\text{cm}^2$. A set of endurance measurements was done for each sample by cycling the capacitors with pulses of different amplitude. Figure 7a presents the polarization loops of the $t = 4.8$ nm film on STO(001), measured at 6.5 MV/cm. The initial polarization increases after 10 cycles due to the wake-up effect discussed above, and additional cycling progressively reduces the polarization. $2P_r$ is plotted against the number of cycles in Figure 7b (red circles). The maximum $2P_r = 16.6 \mu\text{C}/\text{cm}^2$ after 10 cycles decreases to $7.5 \mu\text{C}/\text{cm}^2$ after 10^9 cycles, before the capacitor breaks. Therefore, endurance of the capacitor is

limited first by fatigue and finally by breakdown. Figure 7b includes endurance measurements under other electric fields. With high field of 7.6 MV/cm (blue triangles), the initial remanent polarization is greater, $2P_r = 19 \mu\text{C}/\text{cm}^2$, and increases to a maximum value of $22.5 \mu\text{C}/\text{cm}^2$ after 10 cycles. With additional cycles, the capacitor is fatigued, but retains $2P_r = 13.8 \mu\text{C}/\text{cm}^2$ after 10^7 cycles before hard breakdown. For the low cycling field (5.4 MV/cm, black squares), $2P_r$ is low in the pristine state, $8.6 \mu\text{C}/\text{cm}^2$, and wake-up effect persists for around 10^2 cycles. Then $2P_r$ progressively decreases from 11.1 to $3 \mu\text{C}/\text{cm}^2$ after 5×10^{10} cycles, without breakdown. Therefore, the number of cycles without breakdown is strongly extended using a low switching voltage. However, polarization is reduced and the wake-up effect is more persistent under these conditions, while there is not wake-up for enough high poling voltage. This is in agreement with the improved oxygen diffusion and the reduction of wake-up effect in polycrystalline HfO_2 -based films increasing amplitude³⁵ or applied field duration.³⁶⁻³⁷ The polarization loops (Figure 7d) of the $t = 6.3$ nm film, measured at 5.1 MV/cm, show wake-up effect during some cycles, and the maximum $2P_r = 24.8 \mu\text{C}/\text{cm}^2$ after 10 cycles is reduced with more cycles to $2P_r = 2 \mu\text{C}/\text{cm}^2$ after 10^{10} cycles. Endurance is similar for switching field of 4.3 MV/cm (Figure 7e). By increasing the field to 5.8 MV/cm, the initial polarization increases, but hard breakdown occurs after 10^7 cycles. Thicker films do not show wake-up, and polarization decreases continuously with cycling. Hard breakdown takes place in the $t = 8.3$ nm film (Figures 7g and 7h) after 2×10^7 cycles at 5.4 MV/cm or 2×10^9 cycles at 4.9 MV/cm. Breakdown did not occur using a lower switching field of 4.3 or 4.0 MV/cm, but $2P_r$ decreased to $3.4 \mu\text{C}/\text{cm}^2$ after 10^{10} cycles. Finally, the $t = 13$ nm film (Figures 7j and 7k) shows breakdown after 10^9 cycles at 4.0 or 3.6 MV/cm, while for a lower applied field of 3.2 MV/cm the polarization decreased to $2P_r = 2.3 \mu\text{C}/\text{cm}^2$ after 10^7 cycles. Similar strong robustness against breakdown when the switching field is reduced was reported for polycrystalline doped HfO_2 films.³⁸ Breakdown in epitaxial films, however, occurs at much higher fields than in polycrystalline films. The endurance measurements of the La:HZO films on Si(001) are summarized in Figure 8. The influence of the switching voltage on endurance follows the observed dependences of the films on STO(001), although the maximum endurance of films on Si is limited to around 10^9 cycles.

Figure 7 shows that La:HZO films on STO(001) suffer fatigue at all switching voltages, and similar behavior is observed in films on Si(001) (Figure 8). We have investigated the influence of the cycling voltage on fatigue. The normalized endurance (Supporting Information S9) shows

the same percentage decrease, that is, fatigue of each film does not depend on the value of the electric field used to test it. Similar independence of the electric field had been observed in perovskite ferroelectrics,³⁹⁻⁴⁰ and it was proposed that there is an influence of electric field amplitude only for very short cycling pulses.⁴¹ In the case of doped HfO₂ films, both clear dependence on the amplitude of the electric field⁴² and no obvious dependence (as published graphs suggest, since normalized polarization is not usually plotted)^{35, 43} have been reported. The independence of fatigue on switching electric field in the epitaxial La:HZO films allows direct comparison of fatigue in films of different thickness. The normalized polarization of the La:HZO films on STO(001) (Figure 9a) and Si(001) (Figure 9b) shows little thickness dependence on fatigue. In contrast, a monotonic increase of fatigue with thickness was reported of undoped epitaxial films.²² Therefore, doping with La mitigates the degradation of endurance of ferroelectric hafnia with increasing thickness. Increasing thickness, the minority monoclinic phase increases for both La-doped and undoped HZO epitaxial films, but the amount is smaller in the La-doped films. This suggests that the reduction of paraelectric phase could be a relevant factor to mitigate fatigue (Figure 9b) and improve endurance (Figure 9d).

The endurance study summarized in Figure 7 includes the current leakage as a function of the number of cycles. The evolution of leakage during the cycling of the $t = 4.8, 6.3, 8.3$ and 13 nm films is presented in Figures 7c, 7f, 7i and 7l, respectively. Leakage remains constant for a certain number of cycles, but increases sharply by several orders of magnitude after a threshold. The defects generated by cycling probably accumulate at the boundaries between the grains and the crystal variants. The observed threshold in the number of cycles suggests that the new defects only have an impact on the leakage when their density is high enough to allow percolation. The threshold occurs in each sample at a lower number of cycles as the switching voltage is higher (Figure 9c). Moreover, the leakage current increases after fewer cycles with a similar electric field as the film becomes thicker. On the other hand, the dependence of $2P_r$ on the number of cycles in Figure 7 shows that hard breakdown (marked with empty symbols) occurs after fewer cycles and a smaller switching electric field as the films becomes thicker. This is evidenced in Figure 9d, where the endurance of the four films is plotted as a function of the switching field. A similar thickness dependence had been observed in polycrystalline HZO films,⁴⁴ although breakdown fields in epitaxial films are much higher. In epitaxial La:HZO films, endurance was limited by

hard breakdown (open symbols), in most tested capacitors. However, in capacitors switched with a low electric field, the low polarization of fatigued capacitors (solid symbols) limits endurance.

Polarization loops generally show different E_c on the negative and positive axes. The imprint field (E_{imp}) of the films on STO(001) is represented as a function of the number of cycles in Figure 10. The dependences indicate that E_{imp} is not only caused by the different work function of the Pt and LSMO electrode. An inhomogeneous distribution of oxygen vacancies can create an internal field that would increase the Schottky barrier height at one interface and decrease it at the other. The loops of the two thickest films ($t = 8.3$ nm and 13 nm) are displaced towards the negative axis of the electric field, with the E_{imp} directed from the upper Pt towards the lower LSMO electrode. The E_{imp} , around 300 kV/cm, decreases with the number of cycles, up to 130 kV/cm in the $t = 8.3$ nm film (blue up triangles) and up to negligible imprint in the $t = 13$ nm film (green down triangles). The behavior clearly differs in the two thinnest films, in which the E_{imp} in the pristine state is directed from the lower LSMO towards the upper Pt electrode, its magnitude being close to 400 and 200 kV/cm in $t = 4.8$ and 6.3 nm films, respectively. After 10 cycles, the E_{imp} reverses its direction. In the $t = 6.3$ nm film (red circles) $E_i \sim 300$ kV/cm decreases to less than 100 kV/cm after 10^{10} cycles, while in the $t = 4.8$ nm film (black squares) the smallest $E_i \sim 80$ kV/cm quickly decreases to almost vanish during additional cycling. There is a correlation between the large E_{imp} in the two thinnest films in their pristine state that decreased rapidly after only about 10 cycles and the wake-up effect of these samples. In general, wake-up is considered to be caused by oxygen vacancies diffusing under the action of the electric field, allowing domain depinning and increased polarization.^{4, 35-36} E_{imp} in the pristine state decreases as the vacancies diffuse under the cumulative action of the electric field cycles. Reduction of internal field during wake-up was also observed in polycrystalline hafnia.⁴⁵⁻⁴⁶ In the case of the epitaxial La-doped films on LSMO, pinned dipoles at the interface could be another contribution to E_{imp} in the pristine state, as has been reported for ferroelectric perovskites on LSMO.⁴⁷ These dipoles can pin ferroelectric domains, reducing the overall polarization. The large positive imprint field in the two thinnest La-doped HZO films can be attributed to these interface dipoles, since its magnitude is larger as thinner the ferroelectric layer is. The observed high reduction of imprint field with few cycles in these two thinnest films can be due to charge injection, causing a space charge layer.⁴⁸⁻⁴⁹ It would

cancel the field created by the interfacial dipoles and suppress the pinning of ferroelectric domains, thus waken-up the capacitors.

Figures 11a-d show the polarization retention of the films on STO(001), measured in pristine state at room temperature. Retention of the $t = 4.8$ nm film is highly dependent on the direction of poling, with the remanent polarization extrapolated to 10 years $2 \mu\text{C}/\text{cm}^2$ for positive voltage and $> 10 \mu\text{C}/\text{cm}^2$ for negative poling. The asymmetry is less in thicker films, and the extrapolated remanent polarization for both positive and negative poling is high in all films. Data collected at 85°C in representative $t = 8.3$ nm samples on STO and Si are plotted in Figures 11e,f. Data show that the retention is still high at high temperature with extrapolated polarization at 10 years larger than $5 \mu\text{C}/\text{cm}^2$. We have quantified retention by fitting the measured data to the $P_r = P_0 t_d^{-k}$ equation (dashed lines in Figures 11a-d), where t_d refers to the time after poling.⁵⁰⁻⁵¹ The graph of the exponent k against thickness in Figure 9g confirms that the asymmetry is much greater in the $t = 4.8$ nm film than in the other films including data measured at 85°C . The corresponding graph for the films on Si(001) is shown in Figure 11h (retention data is in Supporting Information S10). The results confirm the observations on STO: strong asymmetry in the film of thickness less than 5 nm and very long retention in the thicker films for both poling directions. Imprint field, current leakage, and depolarizing field are expected to determine the influence of poling direction and film thickness on retention. Imprint field, critical in the asymmetry, may depend on the presence of monoclinic phase, more important in thicker films, and also on the characteristics of the voltage pulses applied (amplitude, time and polarity).⁷ Current leakage decreases monotonically with thickness, which favors a better retention in thicker films. However, the effect of leakage depends on spatial inhomogeneities, mainly due to grain boundaries, and on the possible coexistence of electronic and ionic contributions with different time scales. Finally, thinner films should be more unstable due to the larger depolarization field, although their larger E_c will have the opposite effect. Nevertheless, the excellent properties of the epitaxial La doped HZO films are achieved with endurance that exceeds 10^{10} cycles, and the films simultaneously exhibit good retention for more than 10 years under the same poling voltage (Supporting Information S11). The poling voltage of around 3 V can allow the use of the capacitors in a ferroelectric random access memory.⁵²

CONCLUSIONS

In conclusion, orthorhombic La-doped HZO films have been epitaxially grown on STO(001) and Si(001) substrates, and their main ferroelectric properties (polarization, endurance and retention) have been determined. Doping does not reduce the E_c of HZO epitaxial films, but the leakage current is substantially reduced. Ferroelectric polarization, particularly in films over 10 nm thick, is greater than that of undoped films. The wake-up effect, a serious drawback in polycrystalline La-doped films, is limited to approximately 100 cycles in epitaxial films and only occurs in thinner films. The films exhibit fatigue, but endurance exceeds 10^{10} cycles, and the films simultaneously exhibit very high retention for more than 10 years. This demonstrates that there is not an intrinsic dilemma between endurance and retention in La-doped HZO films.

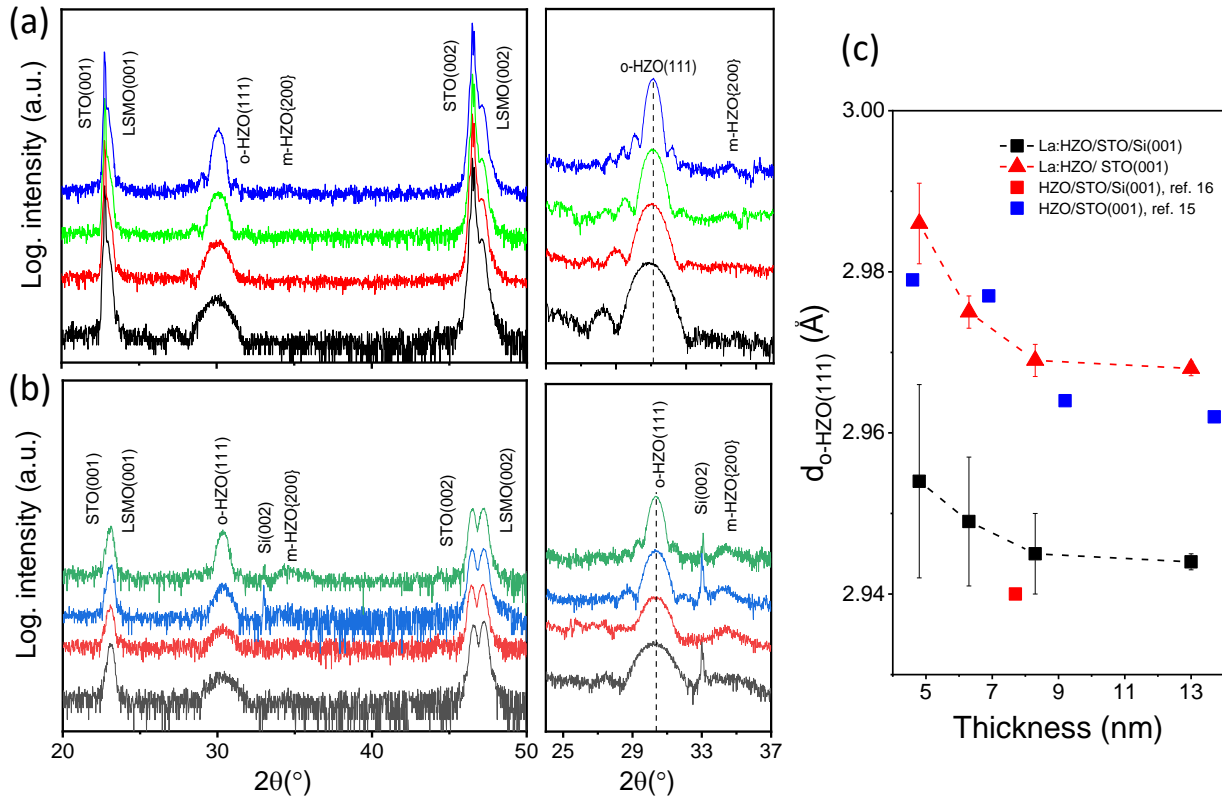


Figure 1. XRD θ - 2θ scans of La:HZO films on (a) LSMO/STO(001) and (b) LSMO/STO/Si(001). Right panels: scans acquired with longer time. (c) Out-of-plane o-HZO(111) lattice distance of La:HZO films on LSMO/STO(001) (red triangles) and LSMO/STO/Si(001) (black squares), plotted as a function of thickness. Out-of-plane lattice distance values of epitaxial undoped HZO on LSMO/STO(001) (blue squares)¹⁵ and LSMO/STO/Si(001) (red square)¹⁶ are plotted for comparison.

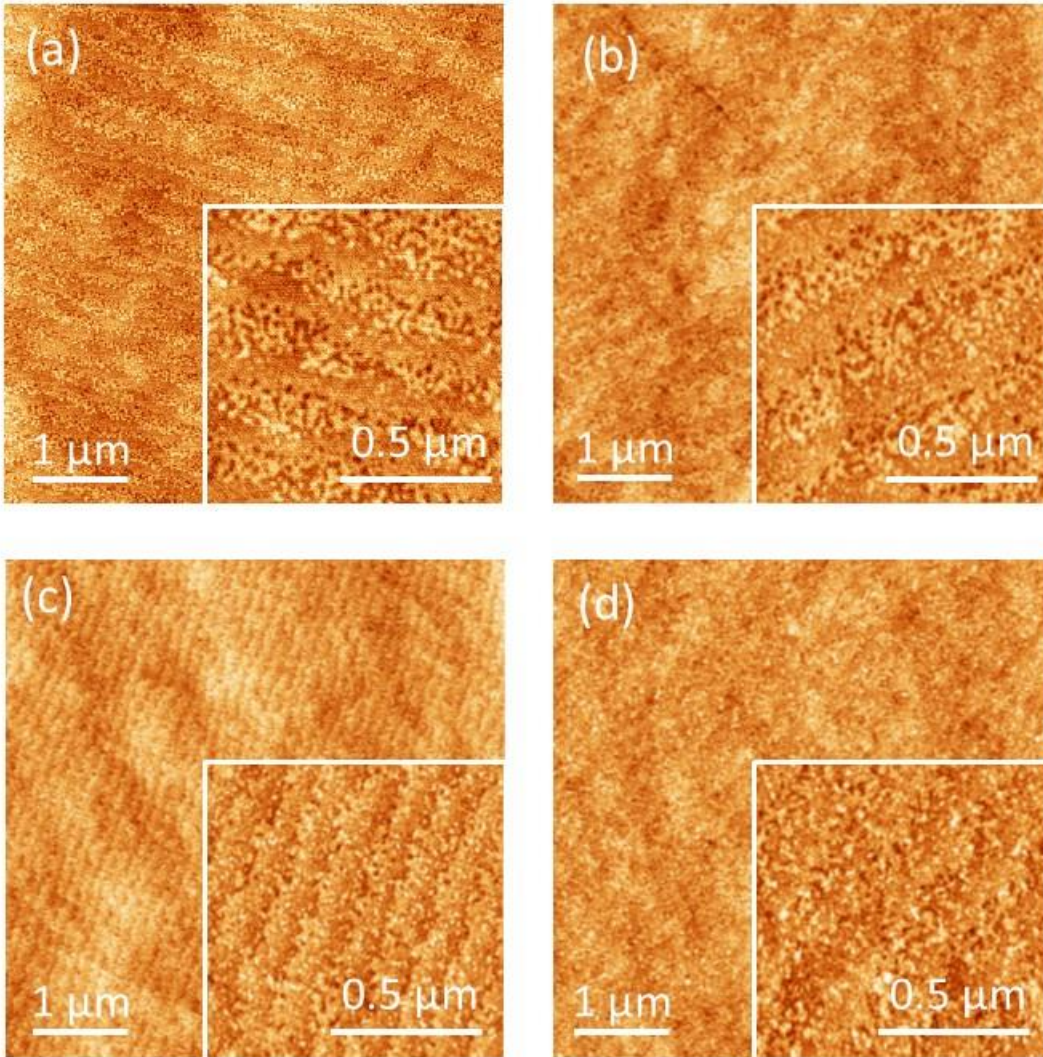


Figure 2. 5 μm x 5 μm AFM topographic images of (a) $t = 4.8$ nm, (b) $t = 6.3$ nm, (c) $t = 8.3$ nm, and (d) $t = 13$ nm films on STO(001). Insets: topographic images of 1 μm x 1 μm scanned areas.

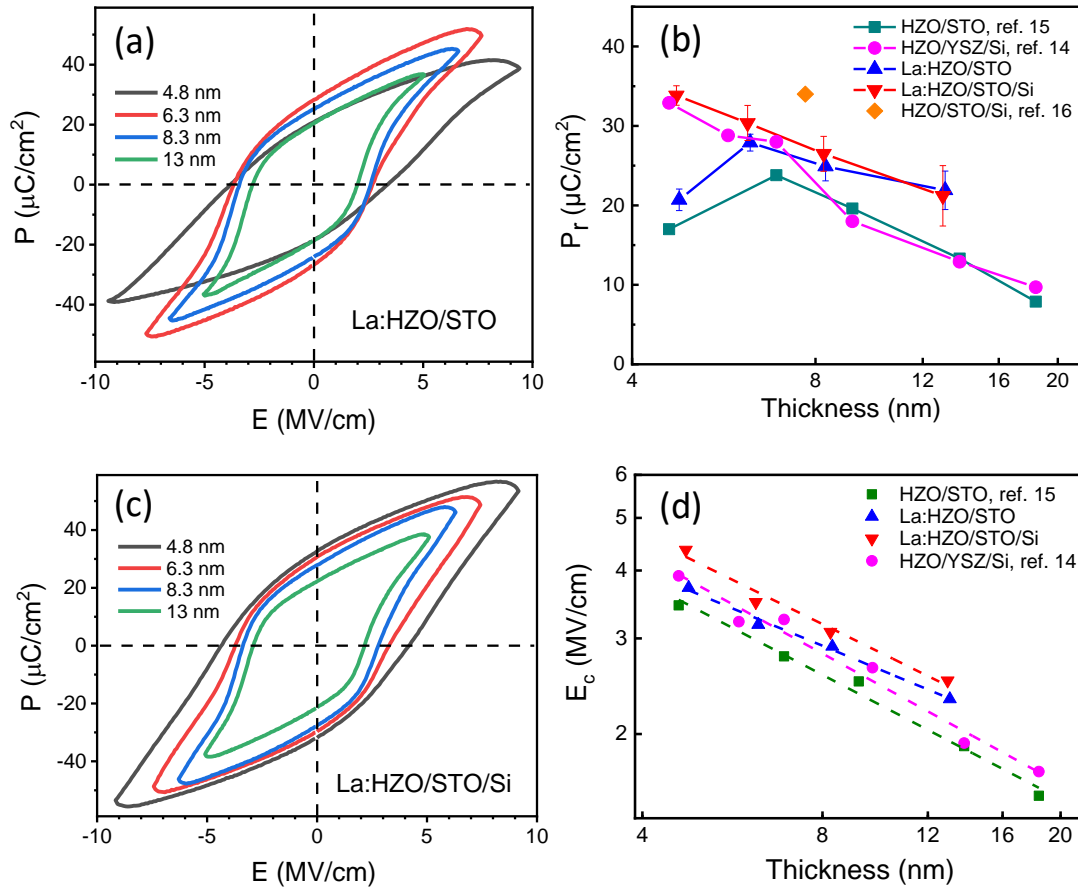


Figure 3. Polarization loops of La:HZO films on STO(001) (a) and Si(001) (c). Dependence of remanent polarization (b) and coercive field (d) on thickness for La:HZO films on STO(001) (blue up triangles) and Si(001) (red down triangles). Data reported for epitaxial undoped HZO films on STO(001) (green squares) and YSZ-buffered Si(001) (pink circles) are included. Error bar on remanent polarization corresponds to the standard deviation among around 10 different measured capacitors.

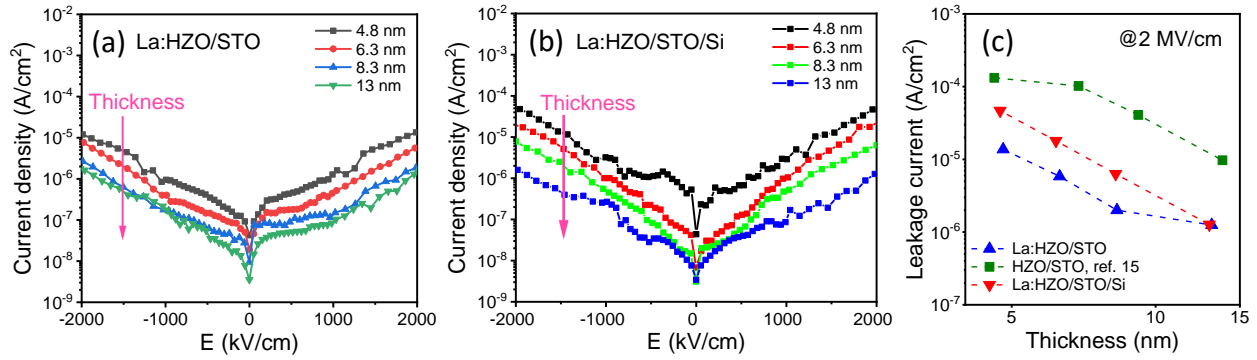


Figure 4. Leakage current of La:HZO films on (a) STO(001) and (b) Si(001). (c) Dependence of leakage current on thickness for La:HZO films on STO(001) (blue up triangles) and Si(001) (red down triangles). Reported data for epitaxial undoped HZO films on STO(001) (green squares) is included.

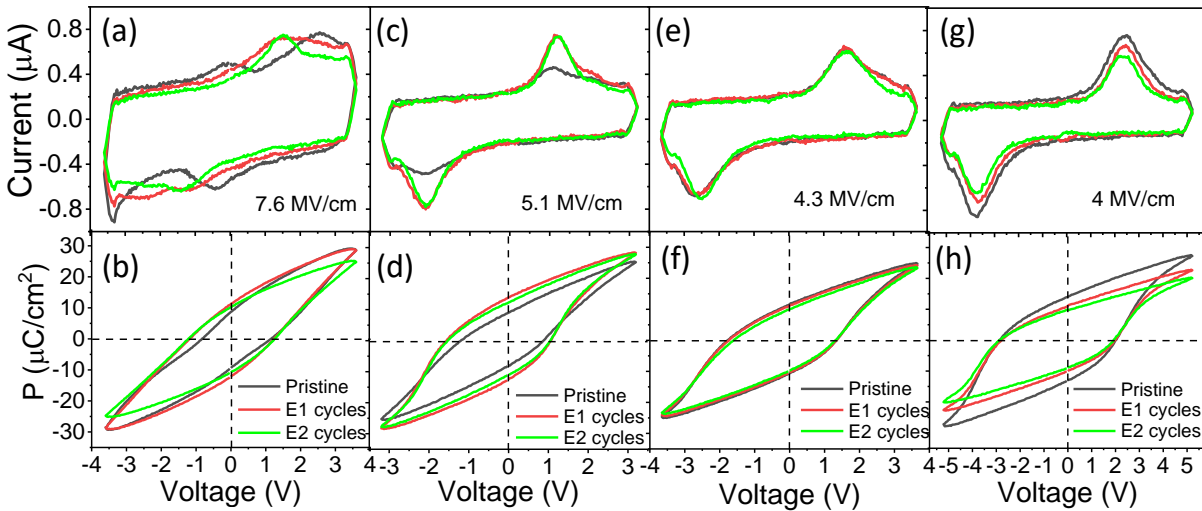


Figure 5. (a) Current - voltage (I-V) curves measured in pristine state and after 10 and 100 cycles and (b) corresponding polarization - voltage (P-V) loops for the $t = 4.8$ nm film on STO(001). I-V curves and P-V loops for the $t = 6.3, 8.3$ and 13 nm films are shown in panels (c-d), (e-f) and (g-h), respectively.

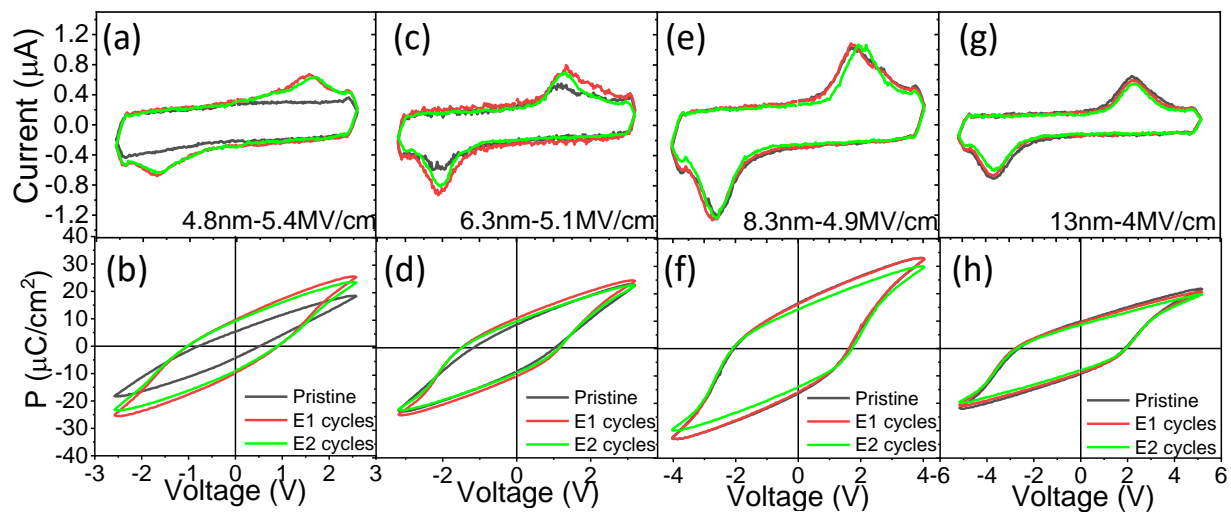


Figure 6. (a) Current - voltage (I-V) curves measured in pristine state and after 10 and 100 cycles and (b) corresponding polarization - voltage (P-V) loops for the $t = 4.8$ nm film on Si(001). I-V curves and P-V loops for the $t = 6.3$, 8.3 and 13 nm films are shown in panels (c-d), (e-f) and (g-h), respectively.

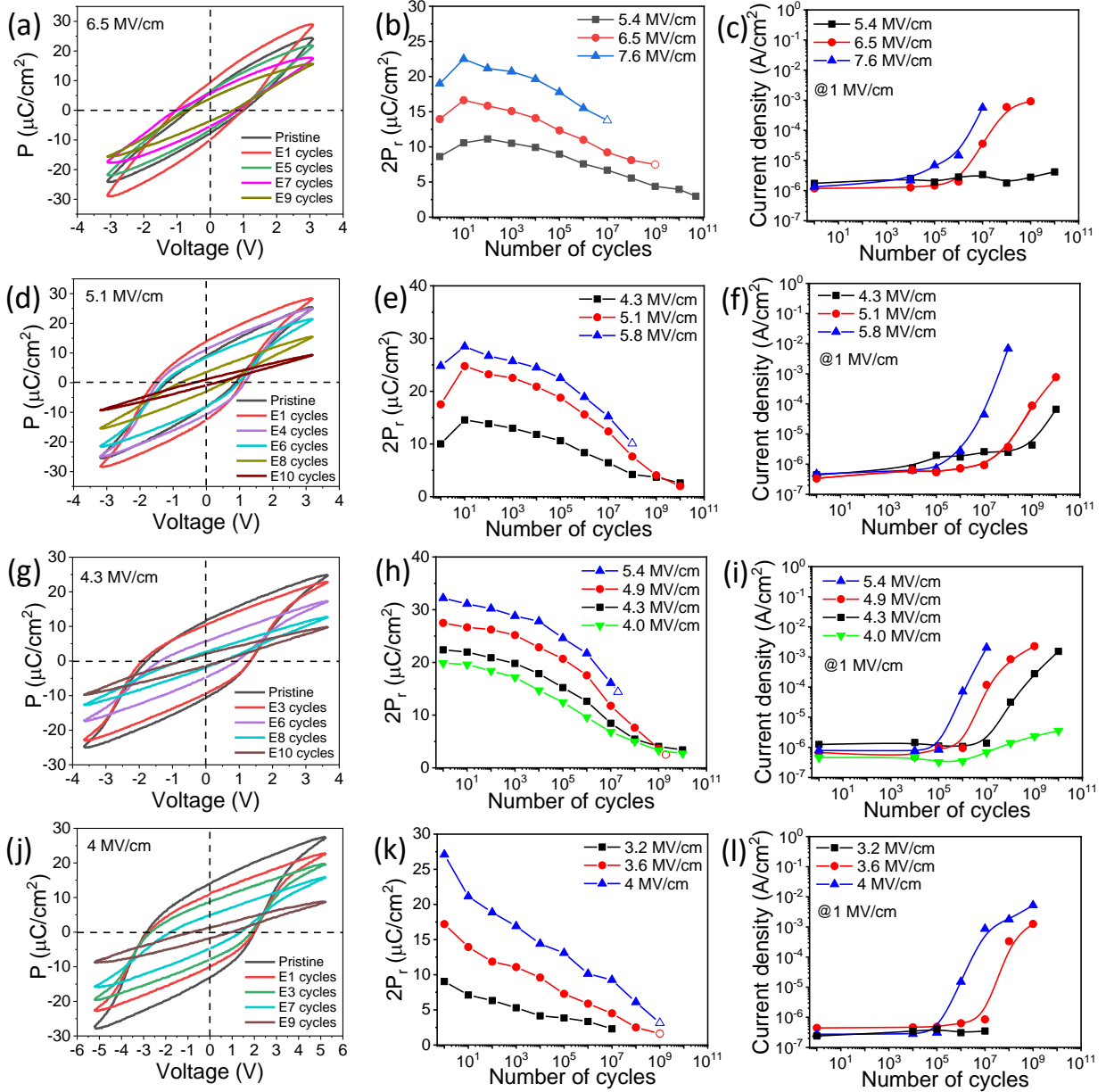


Figure 7. (a) Polarization - voltage P-V loops, (b) endurance and (c) evolution of current leakage with number of cycles for the $t = 4.8$ nm film on STO(001). The P-V loops, endurance and evolution of current leakage with number of cycles corresponding to the $t = 6.3$ nm, 8.3 nm and $t = 13$ nm films are shown in panels (d-f), (g-i) and (j-l), respectively. Empty symbols indicates last measured data point before breakdown.

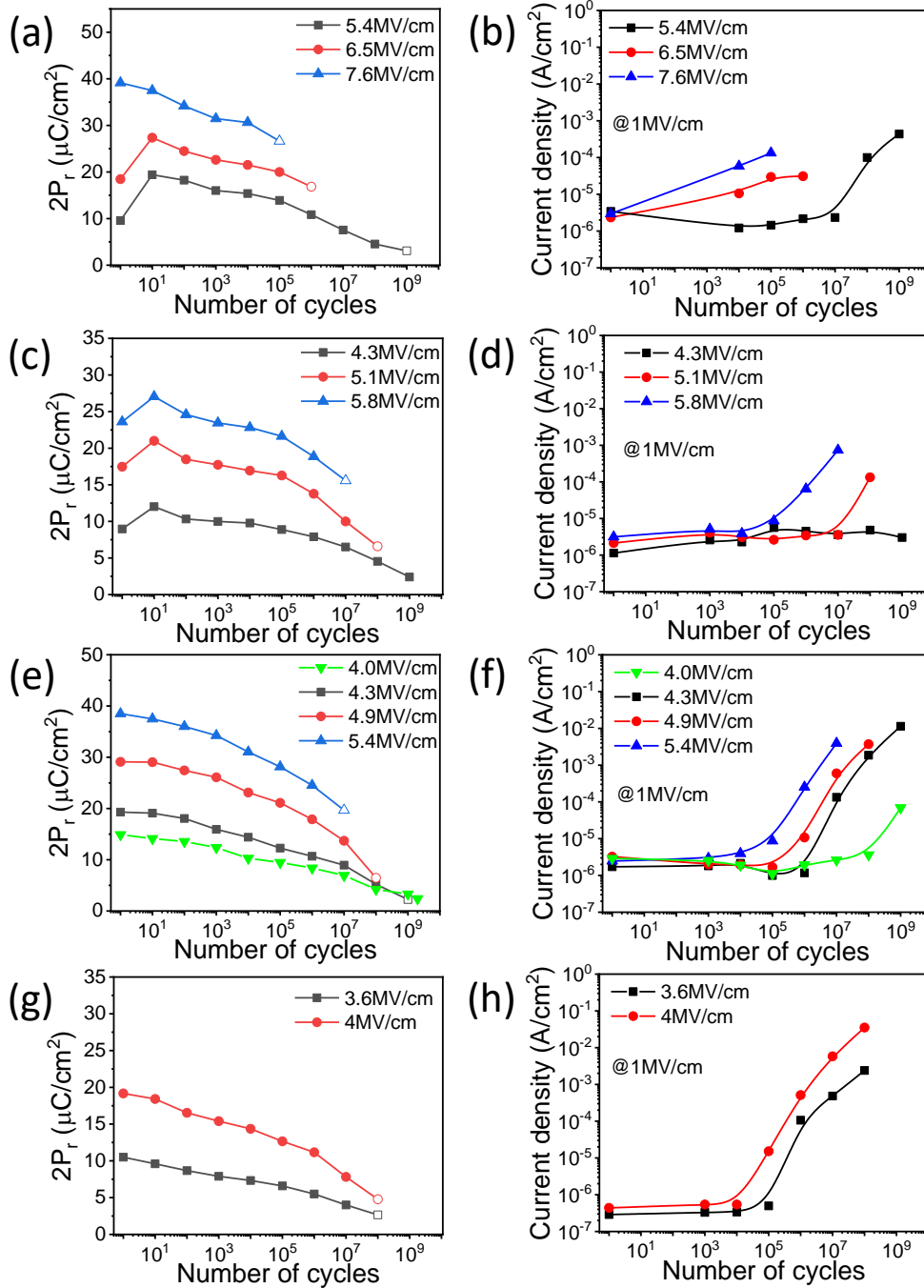


Figure 8. (a) Endurance and (b) variation of current leakage measured at $1 \text{ MV}/\text{cm}$ with number of cycles for the $t = 4.8 \text{ nm}$ film on $\text{Si}(001)$. The endurance and variation of current leakage with number of cycles corresponding to the $t = 6.3 \text{ nm}$, 8.3 nm and $t = 13 \text{ nm}$ films are shown in panels (c-d), (e-f) and (g-h), respectively.

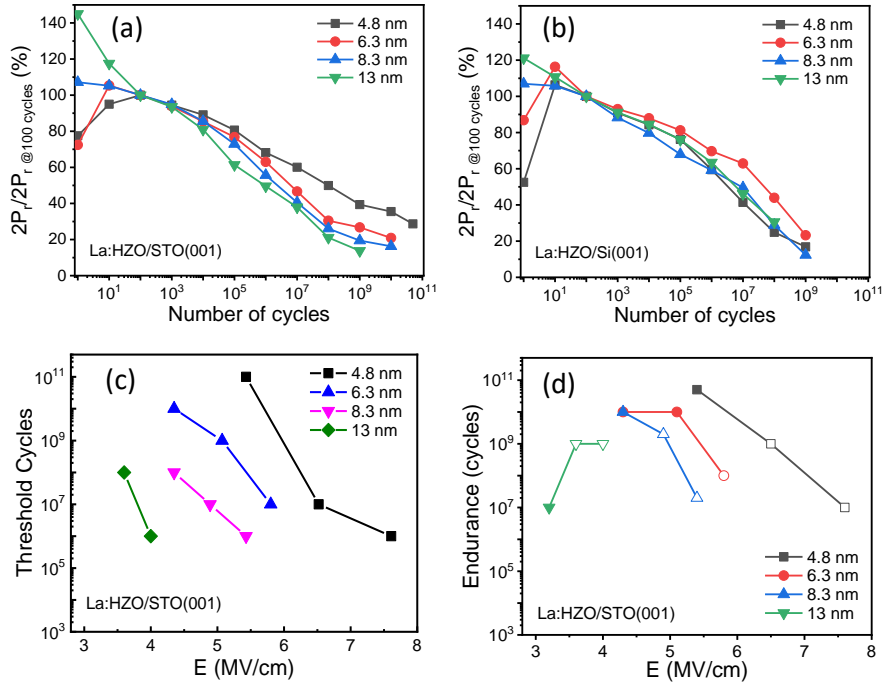


Figure 9. Endurance data normalized to $2P_r$ at 100 cycles of films on (a) STO(001) and (b) Si(001). (c) Map of the threshold of number of cycles for abrupt leakage increase as a function of electric field and thickness of films on STO(001). (d) Map of endurance as a function of electric field and thickness of films on STO(001). Empty symbols denote breakdown.

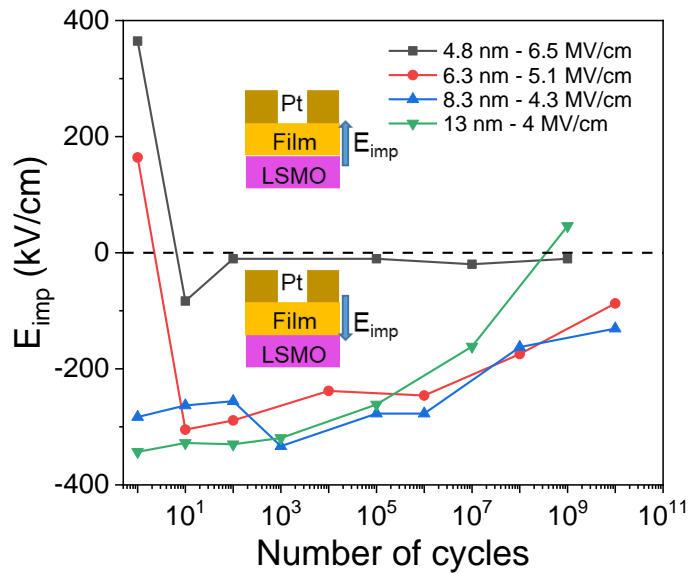


Figure 10. Variation of imprint field (E_{imp}) with the number of cycles for the films on STO(001).

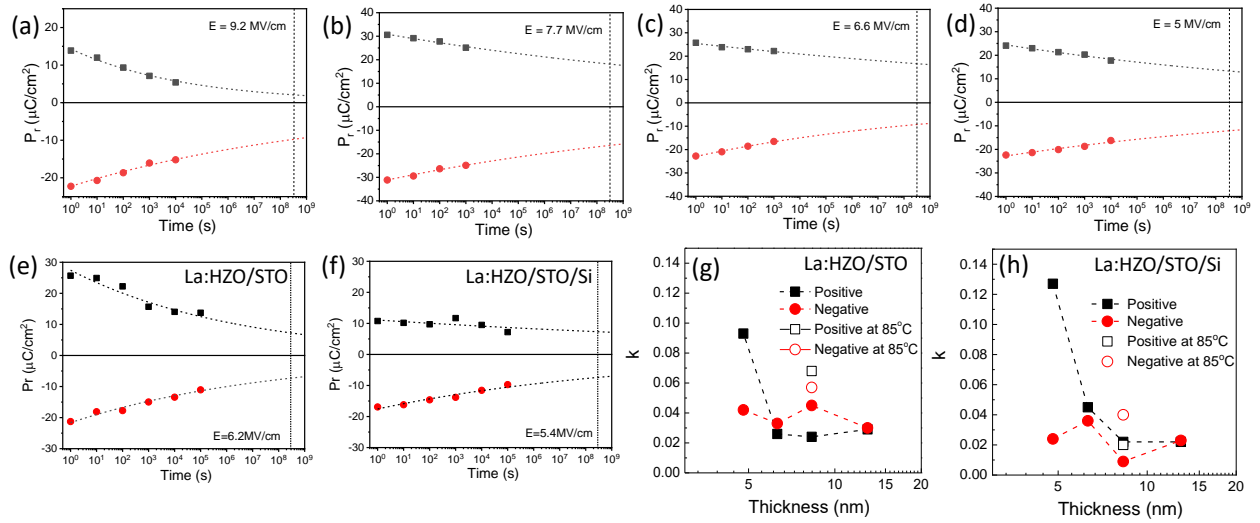


Figure 11. Polarization retention at room temperature of (a) $t = 4.8$ nm, (b) $t = 6.3$ nm, (c) $t = 8.3$ nm and (d) $t = 13$ nm films on STO(001). Polarization retention at 85°C of films with $t = 8.3$ nm on (e) STO(001) and (f) Si(001). Lines are fits to $P_r = P_0 t_d^{-k}$ equation for positive and negative poling. The vertical dashed lines mark a time of 10 years. k parameter plotted for positive and negative poling as a function of thickness for films on (g) STO(001) and (h) Si(001).

Supporting Information.

Simulation of Laue oscillations. XRD pole figures and 2θ - χ frames. Topographic AFM images and height profiles. Polarization loops measured at increasing voltage of films on STO(001) and Si(001). Determination of residual leakage contribution to the polarization loops. Influence of the cycling voltage on fatigue of films on STO(001) and Si(001). Polarization retention of the films on Si(001). Polarization retention of films on STO(001) poled at varying field.

Corresponding Authors

* Ignasi Fina: ifina@icmab.es and Florencio Sánchez: fsanchez@icmab.es

Funding Sources

From the Spanish Ministerio de Ciencia e Innovación, through the “Severo Ochoa” Programme for Centres of Excellence in R&D (SEV-2015-0496) and the MAT2017-85232-R (AEI/FEDER, EU), PID2019-107727RB-I00 (AEI/FEDER, EU), and MAT2015-73839-JIN projects, and Ramón y Cajal contract RYC-2017-22531. From Generalitat de Catalunya (2017 SGR 1377). China Scholarship Council (CSC), grant No. 201807000104.

ACKNOWLEDGMENT

Financial support from the Spanish Ministerio de Ciencia e Innovación, through the “Severo Ochoa” Programme for Centres of Excellence in R&D (SEV-2015-0496) and the MAT2017-85232-R (AEI/FEDER, EU), PID2019-107727RB-I00 (AEI/FEDER, EU), and MAT2015-73839-JIN projects, and from Generalitat de Catalunya (2017 SGR 1377) is acknowledged. IF acknowledges Ramón y Cajal contract RYC-2017-22531. TS is financially supported by China Scholarship Council (CSC) with No. 201807000104. TS work has been done as a part of his Ph.D. program in Materials Science at Universitat Autònoma de Barcelona.

REFERENCES

- (1) Böске, T.; Müller, J.; Bräuhaus, D.; Schröder, U.; Böttger, U. Ferroelectricity in Hafnium Oxide Thin Films. *Appl. Phys. Lett.* **2011**, *99* (10), 102903.
- (2) Park, M. H.; Lee, Y. H.; Kim, H. J.; Kim, Y. J.; Moon, T.; Kim, K. D.; Mueller, J.; Kersch, A.; Schroeder, U.; Mikolajick, T. Ferroelectricity and Antiferroelectricity of Doped Thin HfO₂-Based Films. *Adv. Mater.* **2015**, *27* (11), 1811-1831.
- (3) Mikolajick, T.; Slesazeck, S.; Park, M. H.; Schroeder, U. Ferroelectric Hafnium Oxide for Ferroelectric Random-Access Memories and Ferroelectric Field-Effect Transistors. *MRS Bull.* **2018**, *43* (5), 340-346.
- (4) Park, M. H.; Lee, Y. H.; Mikolajick, T.; Schroeder, U.; Hwang, C. S. Review and Perspective on Ferroelectric HfO₂-Based Thin Films for Memory Applications. *MRS Communications* **2018**, *8* (3), 795-808.
- (5) Chernikova, A. G.; Kozodaev, M. G.; Negrov, D. V.; Korostylev, E. V.; Park, M. H.; Schroeder, U.; Hwang, C. S.; Markeev, A. M. Improved Ferroelectric Switching Endurance of La-Doped Hf_{0.5}Zr_{0.5}O₂ Thin Films. *ACS Appl. Mater. Interfaces* **2018**, *10* (3), 2701-2708.

- (6) Kozodaev, M. G.; Chernikova, A. G.; Korostylev, E. V.; Park, M. H.; Khakimov, R. R.; Hwang, C. S.; Markeev, A. M. Mitigating Wakeup Effect and Improving Endurance of Ferroelectric HfO₂-ZrO₂ Thin Films by Careful La-Doping. *J. Appl. Phys.* **2019**, *125* (3), 034101.
- (7) Mehmood, F.; Hoffmann, M.; Lomenzo, P. D.; Richter, C.; Materano, M.; Mikolajick, T.; Schroeder, U. Bulk Depolarization Fields as a Major Contributor to the Ferroelectric Reliability Performance in Lanthanum Doped Hf_{0.5}Zr_{0.5}O₂ Capacitors. *Adv. Mater. Interfaces* **2019**, *6* (21), 1901180.
- (8) Katayama, K.; Shimizu, T.; Sakata, O.; Shiraishi, T.; Nakamura, S.; Kiguchi, T.; Akama, A.; Konno, T. J.; Uchida, H.; Funakubo, H. Growth of (111)-Oriented Epitaxial and Textured Ferroelectric Y-Doped HfO₂ Films for Downscaled Devices. *Appl. Phys. Lett.* **2016**, *109* (11), 112901.
- (9) Mimura, T.; Shimizu, T.; Uchida, H.; Sakata, O.; Funakubo, H. Thickness-Dependent Crystal Structure and Electric Properties of Epitaxial Ferroelectric Y₂O₃-HfO₂ Films. *Appl. Phys. Lett.* **2018**, *113* (10), 102901.
- (10) Lyu, J.; Fina, I.; Solanas, R.; Fontcuberta, J.; Sánchez, F. Robust Ferroelectricity in Epitaxial Hf_{1/2}Zr_{1/2}O₂ Thin Films. *Appl. Phys. Lett.* **2018**, *113* (8), 082902.
- (11) Li, T.; Zhang, N.; Sun, Z.; Xie, C.; Ye, M.; Mazumdar, S.; Shu, L.; Wang, Y.; Wang, D.; Chen, L. Epitaxial Ferroelectric Hf_{0.5}Zr_{0.5}O₂ Thin Film on a Buffered Ysz Substrate through Interface Reaction. *J. Mater. Chem. C* **2018**, *6* (34), 9224-9231.
- (12) Yoong, H. Y.; Wu, H.; Zhao, J.; Wang, H.; Guo, R.; Xiao, J.; Zhang, B.; Yang, P.; Pennycook, S. J.; Deng, N. Epitaxial Ferroelectric Hf_{0.5}Zr_{0.5}O₂ Thin Films and Their Implementations in Memristors for Brain-Inspired Computing. *Adv. Funct. Mater.* **2018**, *28* (50), 1806037.
- (13) Wei, Y.; Nukala, P.; Salverda, M.; Matzen, S.; Zhao, H. J.; Momand, J.; Everhardt, A. S.; Agnus, G.; Blake, G. R.; Lecoer, P. A Rhombohedral Ferroelectric Phase in Epitaxially Strained Hf_{0.5}Zr_{0.5}O₂ Thin Films. *Nat. Mater.* **2018**, *17* (12), 1095-1100.
- (14) Lyu, J.; Fina, I.; Fontcuberta, J.; Sánchez, F. Epitaxial Integration on Si (001) of Ferroelectric Hf_{0.5}Zr_{0.5}O₂ Capacitors with High Retention and Endurance. *ACS Appl. Mater. Interfaces* **2019**, *11* (6), 6224-6229.
- (15) Lyu, J.; Fina, I.; Solanas, R.; Fontcuberta, J.; Sánchez, F. Growth Window of Ferroelectric Epitaxial Hf_{0.5}Zr_{0.5}O₂ Thin Films. *ACS Appl. Electron. Mater.* **2019**, *1* (2), 220-228.
- (16) Lyu, J.; Fina, I.; Bachelet, R.; Saint-Girons, G.; Estandía, S.; Gázquez, J.; Fontcuberta, J.; Sánchez, F. Enhanced Ferroelectricity in Epitaxial Hf_{0.5}Zr_{0.5}O₂ Thin Films Integrated with Si (001) Using SrTiO₃ Templates. *Appl. Phys. Lett.* **2019**, *114* (22), 222901.
- (17) Estandía, S.; Dix, N.; Gázquez, J.; Fina, I.; Lyu, J.; Chisholm, M. F.; Fontcuberta, J.; Sanchez, F. Engineering Ferroelectric Hf_{0.5}Zr_{0.5}O₂ Thin Films by Epitaxial Stress. *ACS Appl. Electron. Mater.* **2019**, *1* (8), 1449-1457.

- (18) Sulzbach, M. C.; Estandía, S.; Long, X.; Lyu, J.; Dix, N.; Gàzquez, J.; Chisholm, M. F.; Sánchez, F.; Fina, I.; Fontcuberta, J. Unraveling Ferroelectric Polarization and Ionic Contributions to Electroresistance in Epitaxial $\text{Hf}_{0.5}\text{Zr}_{0.5}\text{O}_2$ Tunnel Junctions. *Adv. Electron. Mater.* **2019**, *6*, 1900852.
- (19) Wei, Y.; Matzen, S.; Maroutian, T.; Agnus, G.; Salverda, M.; Nukala, P.; Chen, Q.; Ye, J.; Lecoer, P.; Noheda, B. Magnetic Tunnel Junctions Based on Ferroelectric $\text{Hf}_{0.5}\text{Zr}_{0.5}\text{O}_2$ Tunnel Barriers. *Phys. Rev. Appl.* **2019**, *12* (3), 031001.
- (20) Sulzbach, M. C.; Estandía, S.; Gàzquez, J.; Sánchez, F.; Fina, I.; Fontcuberta, J. Blocking of Conducting Channels Widens Window for Ferroelectric Resistive Switching in Interface-Engineered $\text{Hf}_{0.5}\text{Zr}_{0.5}\text{O}_2$ Tunnel Devices. *Adv. Funct. Mater.* **2020**, *30*, 2002638.
- (21) Estandía, S.; Dix, N.; Chisholm, M. F.; Fina, I.; Sanchez, F. Domain Matching Epitaxy of Ferroelectric $\text{Hf}_{0.5}\text{Zr}_{0.5}\text{O}_2$ (111) on $\text{La}_{2/3}\text{Sr}_{1/3}\text{MnO}_3$ (001). *Crystal Growth & Design* **2020**, *20* (6), 3801-3806.
- (22) Lyu, J.; Song, T.; Fina, I.; Sanchez, F. High Polarization, Endurance and Retention in Sub-5 nm $\text{Hf}_{0.5}\text{Zr}_{0.5}\text{O}_2$ Films. *Nanoscale* **2020**, *12*, 11280-11287.
- (23) Nukala, P.; Wei, Y.; de Haas, V.; Guo, Q.; Antoja-Lleonart, J.; Noheda, B. Guidelines for the Stabilization of a Polar Rhombohedral Phase in Epitaxial $\text{Hf}_{0.5}\text{Zr}_{0.5}\text{O}_2$ Thin Films. *arXiv preprint arXiv:2005.01809* **2020**.
- (24) Cheema, S. S.; Kwon, D.; Shanker, N.; dos Reis, R.; Hsu, S.-L.; Xiao, J.; Zhang, H.; Wagner, R.; Datar, A.; McCarter, M. R.; Serrao, C. R.; Yadav, A. K.; Karbasian, G.; Hsu, C.-H.; Tan, A. J.; Wang, L.-C.; Thakare, V.; Zhang, X.; Mehta, A.; Karapetrova, E.; Chopdekar, R. V.; Shafer, P.; Arenholz, E.; Hu, C.; Proksch, R.; Ramesh, R.; Ciston, J.; Salahuddin, S. Enhanced Ferroelectricity in Ultrathin Films Grown Directly on Silicon. *Nature* **2020**, *580* (7804), 478-482.
- (25) Li, T.; Ye, M.; Sun, Z.; Zhang, N.; Zhang, W.; Inguva, S.; Xie, C.; Chen, L.; Wang, Y.; Ke, S. Origin of Ferroelectricity in Epitaxial Si-Doped HfO_2 Films. *ACS Appl. Mater. Interfaces* **2019**, *11* (4), 4139-4144.
- (26) Lee, H. N.; Nakhmanson, S. M.; Chisholm, M. F.; Christen, H. M.; Rabe, K. M.; Vanderbilt, D. Suppressed Dependence of Polarization on Epitaxial Strain in Highly Polar Ferroelectrics. *Phys. Rev. Lett.* **2007**, *98* (21), 217602.
- (27) Scigaj, M.; Dix, N.; Fina, I.; Bachelet, R.; Warot-Fonrose, B.; Fontcuberta, J.; Sanchez, F. Ultra-Flat BaTiO_3 Epitaxial Films on $\text{Si}(001)$ with Large out-of-Plane Polarization. *Appl. Phys. Lett.* **2013**, *102* (11), 112905
- (28) McDaniel, M. D.; Ngo, T. Q.; Hu, S.; Posadas, A.; Demkov, A. A.; Ekerdt, J. G. Atomic Layer Deposition of Perovskite Oxides and Their Epitaxial Integration with Si, Ge, and Other Semiconductors. *Applied Physics Reviews* **2015**, *2* (4), 041301.
- (29) Sánchez, F.; Ocal, C.; Fontcuberta, J. Tailored Surfaces of Perovskite Oxide Substrates for Conducted Growth of Thin Films. *Chem. Soc. Rev.* **2014**, *43* (7), 2272-2285.

- (30) Meyer, R.; Waser, R.; Prume, K.; Schmitz, T.; Tiedke, S. Dynamic Leakage Current Compensation in Ferroelectric Thin-Film Capacitor Structures. *Appl. Phys. Lett.* **2005**, *86* (14), 142907.
- (31) Fina, I.; Fabrega, L.; Langenberg, E.; Marti, X.; Sanchez, F.; Varela, M.; Fontcuberta, J. Nonferroelectric Contributions to the Hysteresis Cycles in Manganite Thin Films: A Comparative Study of Measurement Techniques. *J. Appl. Phys.* **2011**, *109* (7), 074105
- (32) González-Casal, S.; Fina, I.; Sánchez, F.; Fontcuberta, J. Direct Reversible Magnetoelectric Coupling in a Ferroelectric/Ferromagnetic Structure Controlled by Series Resistance Engineering. *ACS Appl. Electron. Mater.* **2019**, *1* (9), 1937-1944.
- (33) Dawber, M.; Chandra, P.; Littlewood, P.; Scott, J. Depolarization Corrections to the Coercive Field in Thin-Film Ferroelectrics. *J. Phys.: Condens. Matter* **2003**, *15* (24), L393.
- (34) Migita, S.; Ota, H.; Yamada, H.; Shibuya, K.; Sawa, A.; Toriumi, A. Polarization Switching Behavior of Hf–Zr–O Ferroelectric Ultrathin Films Studied through Coercive Field Characteristics. *Jpn. J. Appl. Phys.* **2018**, *57* (4S), 04FB01.
- (35) Fengler, F. P.; Nigon, R.; Muralt, P.; Grimley, E. D.; Sang, X.; Sessi, V.; Hentschel, R.; LeBeau, J. M.; Mikolajick, T.; Schroeder, U. Analysis of Performance Instabilities of Hafnia-Based Ferroelectrics Using Modulus Spectroscopy and Thermally Stimulated Depolarization Currents. *Adv. Electron. Mater.* **2018**, *4* (3), 1700547.
- (36) Starschich, S.; Menzel, S.; Böttger, U. Evidence for Oxygen Vacancies Movement During Wake-up in Ferroelectric Hafnium Oxide. *Appl. Phys. Lett.* **2016**, *108* (3), 032903.
- (37) Starschich, S.; Menzel, S.; Böttger, U. Pulse Wake-up and Breakdown Investigation of Ferroelectric Yttrium Doped HfO₂. *J. Appl. Phys.* **2017**, *121* (15), 154102.
- (38) Schroeder, U.; Mueller, S.; Mueller, J.; Yurchuk, E.; Martin, D.; Adelmann, C.; Schloesser, T.; van Bentum, R.; Mikolajick, T. Hafnium Oxide Based Cmos Compatible Ferroelectric Materials. *ECS Journal of Solid State Science and Technology* **2013**, *2* (4), N69-N72.
- (39) Pawlaczyk, C.; Tagantsev, A.; Brooks, K.; Reaney, I.; Klissurska, R.; Setter, N. Fatigue, Rejuvenation and Self-Restoring in Ferroelectric Thin Films. *Integr. Ferroelectr.* **1995**, *9* (4), 293-316.
- (40) Colla, E.; Tagantsev, A.; Kholkin, A.; Setter, N. Dc-Voltage and Cycling Induced Recovery of Switched Polarisation in Fatigued Ferroelectric Thin Films. *Integr. Ferroelectr.* **1995**, *10* (1-4), 289-294.
- (41) Tagantsev, A. K.; Stolichnov, I.; Colla, E.; Setter, N. Polarization Fatigue in Ferroelectric Films: Basic Experimental Findings, Phenomenological Scenarios, and Microscopic Features. *J. Appl. Phys.* **2001**, *90* (3), 1387-1402.
- (42) Huang, F.; Chen, X.; Liang, X.; Qin, J.; Zhang, Y.; Huang, T.; Wang, Z.; Peng, B.; Zhou, P.; Lu, H. Fatigue Mechanism of Yttrium-Doped Hafnium Oxide Ferroelectric Thin Films Fabricated by Pulsed Laser Deposition. *Phys. Chem. Chem. Phys.* **2017**, *19* (5), 3486-3497.

- (43) Liu, X.; Zhou, D.; Guan, Y.; Li, S.; Cao, F.; Dong, X. Endurance Properties of Silicon-Doped Hafnium Oxide Ferroelectric and Antiferroelectric-Like Thin Films: A Comparative Study and Prediction. *Acta Mater.* **2018**, *154*, 190-198.
- (44) Walters, G.; Shekhawat, A.; Rudawski, N. G.; Moghaddam, S.; Nishida, T. Tiered Deposition of Sub-5 nm Ferroelectric $\text{Hf}_{1-x}\text{Zr}_x\text{O}_2$ Films on Metal and Semiconductor Substrates. *Appl. Phys. Lett.* **2018**, *112* (19), 192901.
- (45) Park, M.; Kim, H.; Kim, Y.; Moon, T.; Kim, K.; Lee, Y.; Hyun, S.; Hwang, C. Study on the Internal Field and Conduction Mechanism of Atomic Layer Deposited Ferroelectric $\text{Hf}_{0.5}\text{Zr}_{0.5}\text{O}_2$ Thin Films. *J. Mater. Chem. C* **2015**, *3* (24), 6291-6300.
- (46) Pešić, M.; Fengler, F. P. G.; Larcher, L.; Padovani, A.; Schenk, T.; Grimley, E. D.; Sang, X.; LeBeau, J. M.; Slesazek, S.; Schroeder, U. Physical Mechanisms Behind the Field-Cycling Behavior of HfO_2 -Based Ferroelectric Capacitors. *Adv. Funct. Mater.* **2016**, *26* (25), 4601-4612.
- (47) Yu, P.; Chu, Y.-H.; Ramesh, R. Oxide Interfaces: Pathways to Novel Phenomena. *Mater. Today* **2012**, *15* (7-8), 320-327.
- (48) Kim, Y.-M.; Morozovska, A.; Eliseev, E.; Oxley, M. P.; Mishra, R.; Selbach, S. M.; Grande, T.; Pantelides, S. T.; Kalinin, S. V.; Borisevich, A. Y. Direct Observation of Ferroelectric Field Effect And vacancy-Controlled Screening at the $\text{BiFeO}_3/\text{La}_x\text{Sr}_{1-x}\text{MnO}_3$ Interface. *Nat. Mater.* **2014**, *13*, 1019–1025.
- (49) Tian, B. B.; Liu, Y.; Chen, L. F.; Wang, J. L.; Sun, S.; Shen, H.; Sun, J. L.; Yuan, G. L.; Fusil, S.; Garcia, V. Space-Charge Effect on Electroresistance in Metal-Ferroelectric-Metal Capacitors. *Sci. Rep.* **2015**, *5* (1), 1-9.
- (50) Kim, D.; Jo, J.; Kim, Y.; Chang, Y.; Lee, J.; Yoon, J.-G.; Song, T.; Noh, T. Polarization Relaxation Induced by a Depolarization Field in Ultrathin Ferroelectric BaTiO_3 Capacitors. *Phys. Rev. Lett.* **2005**, *95* (23), 237602.
- (51) Jo, J.; Kim, D.; Kim, Y.; Choe, S.-B.; Song, T.; Yoon, J.-G.; Noh, T. Polarization Switching Dynamics Governed by the Thermodynamic Nucleation Process in Ultrathin Ferroelectric Films. *Phys. Rev. Lett.* **2006**, *97* (24), 247602.
- (52) Eshita, T.; Wang, W.; Nomura, K.; Nakamura, K.; Saito, H.; Yamaguchi, H.; Mihara, S.; Hikosaka, Y.; Kataoka, Y.; Kojima, M. Development of Highly Reliable Ferroelectric Random Access Memory and Its Internet of Things Applications. *Jpn. J. Appl. Phys.* **2018**, *57* (11S), 11UA01.